Stem Cell Reports
Resource
ISSCR
OPEN ACCESS

Fluorescent Gene Tagging of Transcriptionally Silent Genes in hiPSCs

Brock Roberts,[1] Melissa C. Hendershott,[1] Joy Arakaki,[1] Kaytlyn A. Gerbin,[1] Haseeb Malik,[1] Angelique Nelson,[1] Jamie Gehring,[1] Caroline Hookway,[1] Susan A. Ludmann,[1] Ruian Yang,[1] Amanda Haupt,[1] Tanya Grancharova,[1] Veronica Valencia,[1] Margaret A. Fuqua,[1] Andrew Tucker,[1] Susanne M. Rafelski,[1] and Ruwanthi N. Gunawardane[1,*]
[1]Allen Institute for Cell Science, Seattle, WA 98109, USA
*Correspondence: rug@alleninstitute.org
https://doi.org/10.1016/j.stemcr.2019.03.001

SUMMARY

We describe a multistep method for endogenous tagging of transcriptionally silent genes in human induced pluripotent stem cells (hiPSCs). A monomeric EGFP (mEGFP) fusion tag and a constitutively expressed mCherry fluorescence selection cassette were delivered in tandem via homology-directed repair to five genes not expressed in hiPSCs but important for cardiomyocyte sarcomere function: *TTN*, *MYL7*, *MYL2*, *TNNI1*, and *ACTN2*. CRISPR/Cas9 was used to deliver the selection cassette and subsequently mediate its excision via microhomology-mediated end-joining and non-homologous end-joining. Most excised clones were effectively tagged, and all properly tagged clones expressed the mEGFP fusion protein upon differentiation into cardiomyocytes, allowing live visualization of these cardiac proteins at the sarcomere. This methodology provides a broadly applicable strategy for endogenously tagging transcriptionally silent genes in hiPSCs, potentially enabling their systematic and dynamic study during differentiation and morphogenesis.

INTRODUCTION

Genome editing has revolutionized cell biology with the ability to precisely edit and engineer genes of interest at endogenous loci (Dambournet et al., 2014, 2018; Doyon et al., 2011; Grassart et al., 2014; Mahen et al., 2014; Otsuka et al., 2016; Roberts et al., 2017). Editing human induced pluripotent stem cells (hiPSCs) provides a particularly powerful model for interrogating cellular organization and dynamics, disease mechanisms, and regeneration in a diploid, non-transformed, and relatively stable genomic context. Differentiating edited hiPSCs into multiple lineages presents an ideal model system for disease modeling and regenerative medicine (Drubin and Hyman, 2017).

We described a CRISPR/Cas9-mediated endogenous gene tagging approach that we used to systematically tag more than 25 different target genes in hiPSCs (Addgene, 2018; Coriell Medical Institute Biorepository, 2018; Haupt et al., 2018; Roberts et al., 2017). The edited cells express targeted proteins under endogenous regulation, bypassing artifacts associated with overexpression systems (Gibson et al., 2013). A key feature of this method is the drug-free enrichment of edited cells by fluorescence-activated cell sorting (FACS), which relies on the expression of the tagged protein. However, target genes of interest that are silent in hiPSCs but expressed in differentiated cells are refractory to this approach. This hurdle can be overcome by delivering constitutively expressed selection markers such as drug resistance and/or fluorescent proteins. The subsequent removal of these selection cassettes from the edited cells has traditionally been achieved with recombinases such as the Cre/Lox system (Skarnes et al., 2011; Yao et al., 2017). This requires the introduction of recombinases to the edited cells and leaves residual sequences (e.g., *LoxP* sites) at the target locus, which may disrupt gene function.

To circumvent this limitation, we developed a CRISPR/Cas9 editing approach incorporating a fluorescent tag into silent loci with potentially no residual sequence (Figure 1A). First, a monomeric EGFP (mEGFP) tag is delivered via homology-directed repair (HDR) in tandem with a constitutively expressed CAGGS:mCherry excisable selection cassette, enabling FACS-based selection of the edited cells. This cassette is then excised in a second step also utilizing Cas9. We include repeat-rich sequences in the donor template that promote excision via the microhomology-mediated end-joining (MMEJ) pathway. Deletion of the excision site leaves an in-frame peptide linker between the coding sequence of the target gene and the fluorescent tag, rather than an undesired genomic scar often associated with recombinases. While some of the effectively tagged clones were products of MMEJ-mediated excision, others resulted from non-homologous end-joining (NHEJ)-mediated excision incorporating the tetrapeptide Pro-Gly-Ser-Gly as part of the linker sequence (Figure 1A, lower box). Therefore the combined contributions of MMEJ and NHEJ result in efficient cassette excision to effectively generate a mEGFP fusion protein.

MMEJ has been used to promote various genome manipulations, including large chromosomal insertions, deletions, and disease-related changes (Bae et al., 2014; Kim et al., 2018; Nakade et al., 2014; Sakuma et al., 2016; Shen et al., 2018). Our strategy harnesses the MMEJ repair pathway for the purpose of endogenous tagging, and uses

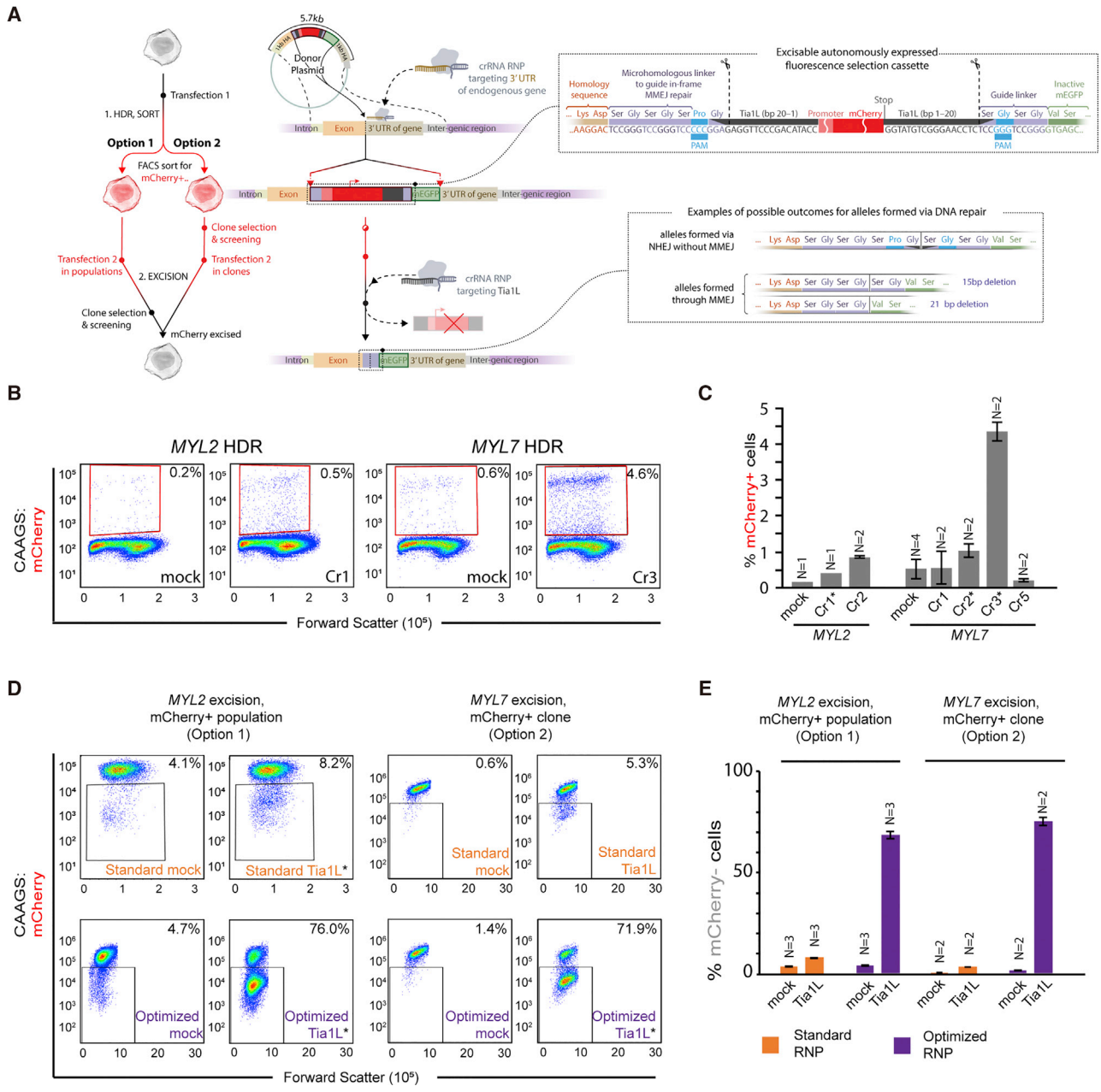

Figure 1. Cas9/HDR-Mediated Delivery and Subsequent Cas9/MMEJ-Mediated Excision of a Constitutively Expressed Selection Cassette Achieves Tagging of Silent Genes

(A) Schematic of tagging approach with *MYL2* donor plasmid as an example. Tia1L protospacers are orientated "PAM-out." Scissor icons indicate positions of anticipated Cas9 cleavage. Options 1 and 2 reflect workflow variations discussed in Results.

(B) FACS sorting of mCherry$^+$ cells after HDR at the *MYL2* and *MYL7* example loci (other loci shown in Figure S1A). Percentages of mCherry$^+$ cells isolated by FACS after transfection with donor plasmids and the indicated duplexed crRNA and wild-type Cas9 RNP are displayed alongside mock transfections with non-targeting crRNA. Boxes indicate gates defining mCherry$^+$ cells for measurement and sorting. The identity of the targeting crRNA is indicated within each plot.

(C) Graphed data from (B) and Figure S1A. Where shown, error is standard deviation (SD) among n technical replicates indicated in the graph. Asterisks indicate populations used to isolate clones. All *MYL7* experiments were from trial 2 (Figure S1A).

(D) Flow-cytometry analysis of mCherry$^-$ cells to measure and recover excised cells. The sorted mCherry$^+$ cells from (B) were expanded and transfected with either mock or Tia1L-specific RNPs for excision of the selection cassette. *MYL2* mCherry$^+$ cell populations (option 1) were transfected for excision while *MYL7* mCherry$^+$ cells were derived from validated, unexcised clones (option 2). RNPs were formulated with

(legend continued on next page)

exogenous MMEJ repair templates designed in the donor template to generate desired fusion protein linkers. We have also used improved gene-editing reagents to achieve excision efficiencies (>50% in optimized experiments, without negative selection) that rival recombinases, resulting in an efficient strategy for successful tagging. We demonstrate this method by introducing an in-frame mEGFP tag to the coding sequence of five transcriptionally silent genes encoding proteins in the cardiomyocyte sarcomere. We observed expression of these tagged proteins during cardiomyocyte differentiation and precise localization in all cases to the intended sarcomeric structures in live cells: the Z disc (*ACTN2*, α-actinin 2), thin filament (*TNNI1*, troponin I1), atrial (*MYL7*, myosin light chain 7), and ventricular (*MYL2*, myosin light chain 2) thick filaments, and the M line (*TTN*, the sarcomere-spanning protein titin, tagged at its C terminus for M-line labeling). Live imaging of these cells bypasses the need to sacrifice samples for fixation, creating cell lines that can be used to study dynamic biological processes in real time in hiPSC- derived cardiomyocytes.

These methods for creating isogenic, tagged hiPSCs may facilitate the study of differentiation-specific proteins in response to environmental, drug, and genetic perturbations in specialized cell types differentiated from hiPSCs. The broadly applicable tagging strategy described here will thus potentially enable various image-based, biochemical, and functional investigations into development, disease, and regeneration.

RESULTS

HDR Targeting with the Excisable Cassette

Donor plasmids contained the intended mEGFP tag flanked by 1-kb locus-specific homology regions and included the following features: (1) a constitutively expressed 3.7-kb CAGGS:mCherry selection cassette to facilitate enrichment of edited (mCherry$^+$) cells after its directed incorporation along with mEGFP via HDR; (2) inverted "PAM-out" Tia1L protospacers absent from the human genome and flanking the selection cassette for excision after initial FACS enrichment such that NHEJ would produce an in-frame mEGFP fusion with a Pro-Gly-Ser-Gly linker (Lackner et al., 2015); (3) microhomology-containing sequences encoding common peptide linker residues to bias excision repair outcomes and delete the residual sequence remaining after Cas9 cleavage (Figure 1A).

We introduced the excisable donor templates into hiPSCs using Cas9 ribonucleoprotein (RNP)-mediated electroporation and multiple synthetic CRISPR RNAs (crRNAs) in parallel transfections (Figure 1A, "Transfection 1") (Lin et al., 2014; Roberts et al., 2017; Haupt et al., 2018). Flow cytometry was used to evaluate the frequency of mCherry$^+$ cells indicative of HDR-mediated editing (Figures 1B, 1C, and S1A–S1D). mCherry$^+$ cells were generally more frequent with gene-specific crRNAs compared with mock transfections, indicating HDR targeting. mCherry$^+$ cells were observed at a frequency (~0.1%–5%) consistent with our previous study tagging genes expressed in pluripotent cells (Roberts et al., 2017). The relatively low rates of HDR often observed in stem cells were overcome by sorting a sufficient number of edited cells (>500) for expansion and clone generation. This was preferred to attempting to improve HDR rates with non-selective chemicals that may adversely affect the health and pluripotency of stem cells. While similar HDR frequencies were observed using PGK and CAGGS promoters, we replaced the PGK promoter used in initial experiments (*TNNI1* and *ACTN2*) with CAGGS for more robust and stable expression of the mCherry cassette (Figures S1A–S1D). We also evaluated two workflows for clone generation before and after excision (options 1 and 2 in Figure 1A). In option 1, mCherry$^+$ cells were sorted, expanded, and excised as a population. The excised mCherry$^-$ cells were resorted, expanded, and used to generate clones and screened for genetic validation of the edit (Figures 2A–2C and 2G). In an alternative workflow (Figure 1A, option 2) intended to identify precisely edited clones (i.e., lacking donor backbone or mutations at the untagged allele) prior to the excision step, mCherry$^+$ cells were enriched via FACS and plated for clonal isolation and screening (*MYL7* and *ACTN2*, Figures 2D–2G). Only precisely edited clones were then subjected to the excision step.

Excision of the mCherry Selection Cassette with CRISPR/Cas9 and NHEJ- and MMEJ-Mediated Repair Outcomes

Populations or clones of sorted mCherry$^+$ cells (options 1 and 2) were transfected with RNP complexes specific to the Tia1L protospacer to excise the mCherry selection cassette. We predicted that successful excision of the selection cassette would create an in-frame fusion of the mEGFP tag at each endogenous locus (Figure 1A) and result in

duplexed crRNA:tracrRNA and wild-type Cas9 ("Standard") or with Synthego sgRNAs and TrueCut Cas9 ("Optimized"), as indicated. Percentages of mCherry-putatively excised cells are indicated within the gated boxes. Black asterisks denote experiments used to derive clonal lines.

(E) Graphed data from (D). Error is SD among n technical replicates indicated in the graph.

See also Figure S1.

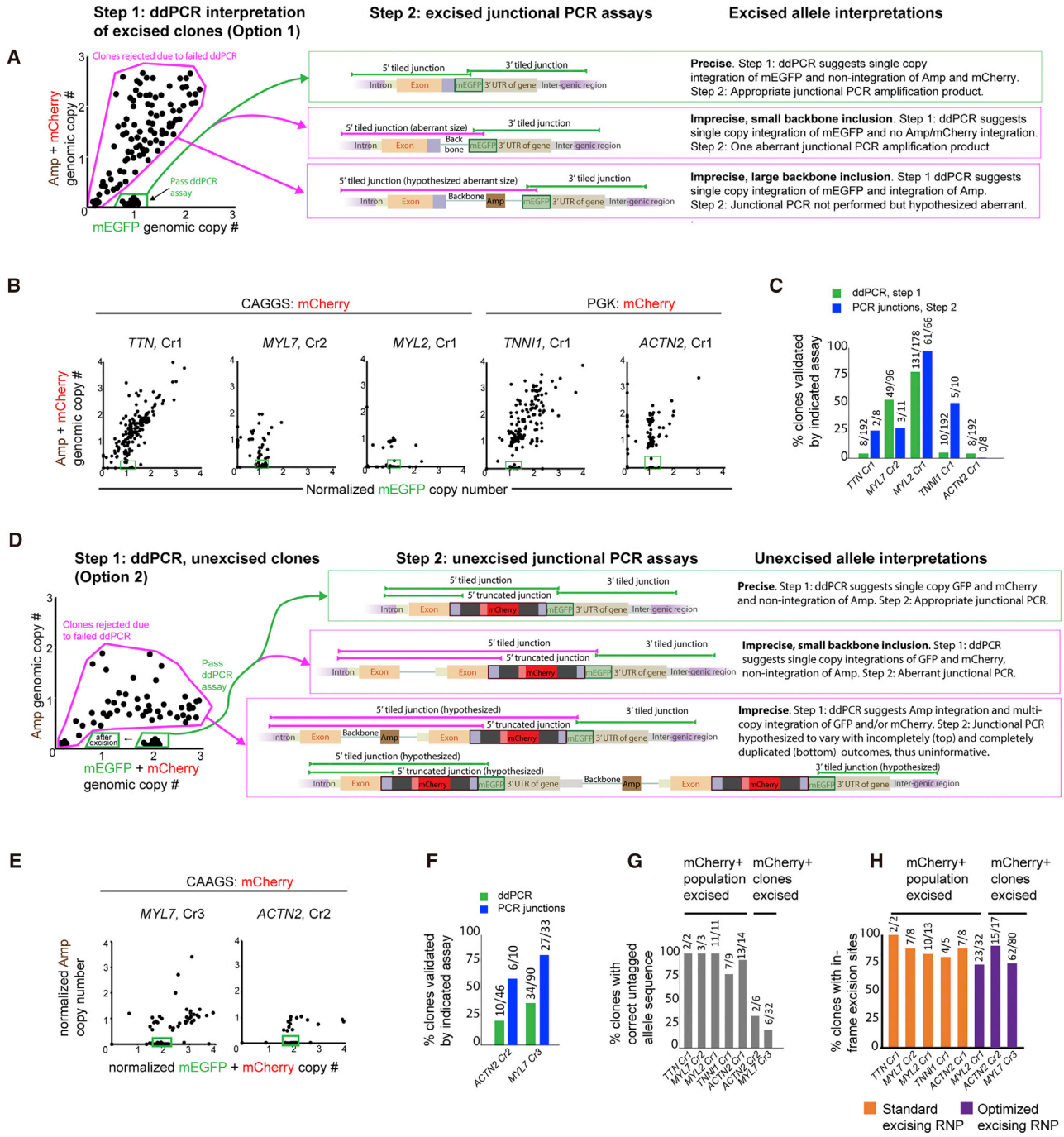

Figure 2. Molecular Assays to Validate Allele Structures within Edited Clones

(A) Schematic illustrating PCR assays identifying precisely tagged, excised clones (Figure 1A, "Option 1"). ddPCR (left, "Step 1") was used to identify clones with mEGFP insertion (normalized genomic mEGFP copy number ~1) and no stable integration of the plasmid or the excised mCherry cassette (additive genomic copy number <0.2) (see Experimental Procedures). Tiled junctional PCR ("Step 2," middle) screening of ddPCR validated clones depicts amplification from frequent precise (green) and imprecise (pink) outcomes.

(B) Normalized genomic copy numbers of the mEGFP, mCherry, and Amp DNA sequences were determined by ddPCR in excised clones, as explained in (A).

(C) Percentages of clones validated according to ddPCR (green) and junctional PCR (blue) assays are shown, among clones tested.

(legend continued on next page)

expression of the tagged fusion protein in differentiated cardiomyocytes. mCherry$^-$ cells indicative of excision appeared within 3 days of transfection, and were up to 9-fold (*MYL7*) more frequent in Tia1L transfected populations compared with mock controls using the standard RNP complex (Figures 1D, 1E, and S1E–S1I). Recovering cells after excision of the PGK:mCherry selection cassette was complicated by decreased mCherry expression over time in mock-excised cells, motivating future experiments with CAGGS:mCherry (Figures S1F and S1H).

RNP complexes composed of the TrueCut Cas9 variant and Synthego modified single guide RNAs (sgRNAs) (hereafter "optimized" RNP complex) greatly improved excision (67%–75% mCherry$^-$ cells) resulting in 16- to 51-fold enrichment of excised cells (Figures 1D, 1E, S1G, and S1I). This optimization rendered subsequent selection of mCherry$^-$ cells by FACS unnecessary. Rather, because they were frequent in the culture, mCherry$^-$ clones were derived from these unenriched, excised populations and analyzed for excision outcomes without sorting.

Molecular Confirmation of Precise mEGFP Tagging and Excision in Isolated Clones

Several PCR assays were used to analyze clonal populations according to our previous screening strategy (Roberts et al., 2017). In brief, droplet digital PCR (ddPCR) was used to screen for single-copy mEGFP integration, absence of donor plasmid backbone integration, and excision or retention of the mCherry sequence (Figures 2A–2F), depending on whether clones were screened before or after excision (Figure 1A, options 1 and 2). Clones identified as candidates for precise editing by ddPCR were further analyzed by junctional PCR (Figures 2A, 2C–2F, S2D, and S2F) and Sanger sequencing (data not shown) to confirm appropriate HDR-mediated incorporation of the tag and/or cassette, depending on workflow. HDR precision varied among the targeted genes with *MYL2* exhibiting the highest frequency of clones without donor plasmid backbone integration at the edited locus as well as the highest frequency with correct PCR junctions (Figures 2B and 2C). We additionally performed Sanger sequencing of the wild-type allele and rejected clones with mutations (Figure 2G).

To evaluate excision precision, we Sanger sequenced the 5′ junction containing the excision site in all excised clones with expected 5′ PCR amplicon product sizes (Table 1). Regardless of the gene targeted, RNP formulation, and workflow used, most excised clones contained sequences consistent with MMEJ and NHEJ outcomes predicted to fuse mEGFP in-frame with the target gene, while frequently deleting the Tia1L protospacer and PAM sequences original to the selection cassette (Figure 2H and Table 1). When excising with the standard Tia1L RNP complex, 83% of clones (n = 36 clones, data from multiple experiments) had tiled junctional sequences predicted to produce a functional fusion protein. Linkers were either consistent with an NHEJ outcome (19% of all outcomes) or MMEJ-driven 6- to 21-bp deletions (64%) resulting in in-frame linkers with different lengths. The optimized excision complex resulted in 92% of clones (n = 98, data combined from multiple experiments) with an in-frame putatively functional fusion protein. Clones derived from excision with the optimized complex also exhibited a preference for MMEJ excision with 51% displaying 3- to 21-bp deletions and 38% consistent with NHEJ (Figure 2H and Table 1; 3% 3- to 9-bp in-frame insertions categorized as neither MMEJ or NHEJ).

To minimize off-target mutations, we targeted protospacers with the fewest predicted off-target sites (Figure S2A). We used the same prediction thresholds as in our previous report targeting expressed genes in which we observed no mutations among 406 high-similarity off-target sites in experiments targeting ten loci (Roberts et al., 2017). *MYL7* was an exception, where we chose

(D) Schematic illustrating PCR assays identifying precisely targeted, unexcised clones (Figure 1A, "Option 2"). ddPCR (left, "Step 1") was used to identify clones with stable insertion of the mEGFP and mCherry sequences (additive normalized copy number ~2) and no stable plasmid integration (genomic copy number <0.2) of the plasmid (see Experimental Procedures). Common allelic outcomes are shown (middle, "Step 2") with tiled junctional PCR assays depicted as in (A). Because the unexcised allele sequence is large, additional confidence in correct editing outcomes was provided when needed by additional amplification of the 5′ truncated junction.

(E) Normalized genomic copy numbers of the mEGFP, mCherry, and Amp DNA sequences were determined by ddPCR in excised clones, as explained in (D).

(F) Percentages of clones validated according to ddPCR (green) and junctional PCR (blue) assays are shown, as in (C).

(G) The percentages of clones with wild-type untagged alleles are shown. *TNNI1* (n = 4) and *ACTN2* (n = 8) clones without validated junctions (C) were screened for NHEJ. 11/62 *MYL2* clones validated by junctions were screened for NHEJ.

(H) The percentage of mCherry$^-$ clones from all excision experiments with in-frame sequenced excision sites (5′ tiled junction) are shown. *MYL2* Cr1 clones excised with the optimized RNP were only analyzed with 5′ junction PCR and sequencing.

In (A) and (D), hypothetical junction outcome examples are depicted in ddPCR-rejected clones despite not performing this assay. This illustrates a potential alternative, ddPCR-independent screening strategy. In (C), (F), (G), and (H), numbers of clones validated and total number screened are indicated fractionally.

See also Figure S2.

Table 1. Sequences of Excision Sites from All Analyzed Clones

RNP Complex	Gene	Allele sequence	outcome	# clones
Standard	TNNI1	TCACAATCCGGGTCCGGGTCCCCCGGATCCGGGTCCGGGGTGAGC	NHEJ	1
		TCACAATCCGGGTCCGGG----------TCCGGGGTGAGC	MMEJ, d15	2
		TCACAATCCGGG----------TCCGGGGTGAGC	MMEJ, d21	1
		TCACAATCCGGGTCCGGGTCCCCCGACATACTCCGGGTCCGGGGTGAGC	i4	1
	ACTN2	GATCTGGTCGACGGGACTGCTGGG----------CCCGGATCCATTGCTACTGTGAGC	MMEJ, d12	7
		GATCTGGATCTGGTCGACGGGACTGCTGGGCCCGGACATATGGGCCCGGATCCATTGCTACTGTGAGC	i2	1
	TTN	TCCATTTCCGGGTCCGGGTCCCCCGGATCCGGGTCCGGGGTGAGC	NHEJ	0
		TCCATTTCCGGGTCCGGG----------GTGAGC	MMEJ, d21	2
	MYL7	GAGGAGGGGTCCGGGTCCCCCGGATCCGGGTCCGGGGTGAGC	NHEJ	2
		GAGGAGGGGTCCGGGTCC----------GGGGTGAGC	MMEJ, d15	2
		GAGGAG----------TCCGGGTCCGGGGTGAGC	MMEJ, d18	2
		GAGGAGGGGTCCGGGTCCCCCGGA------TCCGGGGTGAGC	MMEJ, d6	1
		GAGGAGGGGTCCGGGTCTATATAGGATCCGGGTCCGGGGTGAGC	i2	1
	MYL2	AAGGACTCCGGGTCCGGGTCCCCCGGATCCGGGTCCGGGGTGAGC	MMEJ, NHEJ	4
		AAGGACTCCGGGTCCGGGTCC----------GGGGTGAGC	MMEJ, d15	4
		AAGGACTCCGGGTCCGGGTCCCCCGGATCCGG-TCCGGGGTGAGC	d1	1
		AAGGACTCCGGGTCCGGGTCCCCCGACATAC----------C	d13	1
		AAGGACTCCGGGTCCGGG----------GTGAGC	MMEJ, d21	1
		AAGGACTCCGGGTCCGGGT--------TCCGGGTCCGGGGTGAGCGTGAGC	d8	1
		AAGGACTCCGGGTCCGGGTCC---------GGGTCCGGGGTGAGC	MMEJ, d9	1
			Total	36
			MMEJ, combined	23/36 = **64%**
			NHEJ, combined	7/36 = **19%**
			In-frame, combined	30/36 = **83%**
Optimized	MYL2	AAGGACTCCGGGTCCGGGTCCCCCGGATCCGGGTCCGGGGTGAGC	NHEJ	11
		AAGGACTCCGGGTCCGGGTCC----------GGGGTGAGC	MMEJ, d15	6
		AAGGACTCCGGGTCCGGGTCCCCCGG------GTCCGGGGTGAGC	MMEJ, d6	3
		AAGGACTCCGGGTCCGGG----------GTGAGC	MMEJ, d21	2
		AAGGACTCCGG----------ACTCCGGGTCCGGGGTGAGC	d14	1
		AAGGACTCCGGGTCCGGGTCCCCCGGA-------CCGGGGTGAGC	d7	1
		AAGGACTCCGGGTCCGGGTCCCCCGGA--------CGGGGTGAGC	d8	1
		AAGGACTCCGGGTCCGGGTCCCCGACATACCAATAACTCCGGGTCCGGGGTGAGC	i10	1
		AAGGACTCCGGGTCCGGGTCCCCCGGAGTCTCCGGGTCCGGGGTGAGC	i3	1
		AAGGACTCCGGGTCCGGGTGTTATATAGGTATGTCGGGAACCGGGGTGAGC	i6	1
	ACTN2	GATCTGGTCGACGGGACTGCTGGGCCCGGATCCGGGCCCGGATCCATTGCTACTGTGAGC	NHEJ	6
		GATCTGGTCGACGGGACTGCTGGG----------CCCGGATCCATTGCTACTGTGAGC	MMEJ, d12	6
		GATCTGGTCGACGGGACTGC----------CGGGCCCGGATCCATTGCTACTGTGAGC	MMEJ, d12	3
		GATCTGGTCGACGGGACTGCTGGGCCCGGAGTCCGGGCCCGGATCCATTGCTACTGTGAGC	i1	1
		GATCTGGTCGACGGGCCCAGCAGTCCCGAGTAGGCGCTGAACTTGTGGCCGTTTACGTCGCCGGGCCCGGATCCATT GCTACTGTGAGC	i29	1
	MYL7	GAGGAGGGGTCCGGGTCCCCCGGATCCGGGTCCGGGGTGAGC	NHEJ	20
		GAGGAGGGGTCCGGGTCC----------GGGGTGAGC	MMEJ, d15	24
		GAGGAGGGGTCCGGGTCC----------GGGGTGAGC	MMEJ, d12	2
		GAGGAGGGGTCCGGG----------GTGAGC	MMEJ, d21	2
		GAGGAGGGGTCCGGGTCCCCCGG----------TGAGC	d14	1
		GAGGAGGGGTCCGGGTCCCCCG-A--CATGTCCGGGGTGAGC	MMEJ, d3	1
		GAGGAGGGGTCCGGGTCCCCCGGG------TCCGGGGTGAGC	MMEJ, d6	1
		GAGGAGGGGTCCGGGTCCCCCGGTTCAGCTGAA----------//----------CACAAG	d75	1
		GAGGAGGGGTCCCATACCTTTCATATAGGTATGTCCGGGTCCGGGGTGAGC	i9	1
			Total	98
			MMEJ, combined	50/98 = **51%**
			NHEJ, combined	37/98 = **38%**
			In-frame, combined	90/98 = **92%**

The peptide linker sequence at the excision site was sequenced in all excised clones. All sequences are in the 5′ to 3′ direction. Endogenous protein codons at the C terminus are indicated in orange font. Purple font indicates Pro-Gly-Ser-Gly tetrapeptide motif left from Tia1L PAM and PAM-3 protospacer sequences, predicted to arise from NHEJ repair. Green font indicates beginning of the mEGFP sequence. The size of the deletion or insertion is indicated in red or green font depending on whether mEGFP is in-frame with the endogenous coding sequence (green) or out of frame (red). Frequencies of each allele among sequenced clones are as indicated by parentheses. In-frame alleles resulting from 3- to 6-bp insertions were not classified as MMEJ or NHEJ outcomes but were considered in-frame.

one targeted protospacer (Cr2) with a relatively large number of high-similarity candidate off-target sites. To rule out the possibility of off-target editing at predicted sites, we performed PCR and Sanger sequencing on the 11 highest-similarity predicted off-target loci (Figure S2A, box with alignments) in three *MYL7*-mEGFP clones targeted with Cr2 and found no mutations. We additionally performed exome sequencing on a *TNNI1*-mEGFP clone confirmed to have precise tagging and identified INDELs unique to the edited cell line and absent from the parental WTC cell line background (Figures S2B and S2C). No INDELs attributable to CRISPR/Cas9 cutting and repair were found to exist within 20 bp of candidate off-target digestion sites predicted by a relaxed-parameter search for sites with up to seven mismatches to the *TNNI1* Cr1 or Tia1L crRNA.

Cardiomyocytes Derived from Gene-Edited iPSCs Express Sarcomeric mEGFP Fusion Proteins

We differentiated excised populations and validated clones to evaluate the cardiomyocyte differentiation potential and mEGFP fusion protein expression dynamics and localization in these edited cells. All non-clonal populations (Figure 1A, option 1) excised with the standard RNP complex showed successful cardiomyocyte differentiation with >68% of cells positive for the cardiomyocyte marker cardiac troponin T (cTnT), with a subset (0.2%–16%) of cardiomyocytes expressing mEGFP (Figure 3A). Clones with precise HDR confirmed prior to excision (Figure 1A, option 2), then subsequently excised with the optimized Tia1L RNP and directly differentiated as unsorted populations displayed 36%–62% mEGFP$^+$ cells among cTnT$^+$ cardiomyocytes (Figure 3B, green boxes for examples in left plots; Figure 3C, green bars) and the mEGFP$^+$ cells displayed expected sarcomeric mEGFP localization (Figure 3D). Since these targeted and excised cells were produced within an HDR-validated clonal line (option 2), but did not undergo FACS to accomplish selection for mCherry$^-$ cells due to high excision efficiency (Figures 1D, 1E, 2H, S2E, S2G, and S2I), we focused our flow-cytometry analysis on the subpopulation of excised mCherry$^-$ cardiomyocytes. We observed 68%–76% mEGFP$^+$ cells in mCherry$^-$ cardiomyocytes after excision in these *MYL7* and *ACTN2* clones (Figures 3B and 3C, blue box and blue bars). This was consistent with the high frequency of clones with in-frame excision site sequences at the *MYL7* and *ACTN2* loci (Table 1).

We repeated the differentiation studies in clonal lines for *TNNI1*, *TTN*, *MYL7*, and *ACTN2* that were screened for precise mEGFP fusions at the targeted locus. All four clones displayed cTnT expression (>70% mean cTnT$^+$), spontaneous contraction (data not shown), and mEGFP expression (>89% mEGFP$^+$, among cTnT$^+$) upon differentiation into cardiomyocytes (Figures 4B and 4C; Table S1; Figure S3C). *MYL2*-mEGFP clones also successfully differentiated (Figures 4G, 4H, and S3D) and displayed increased mEGFP expression over time by flow cytometry (Figures 4G, 4H, and S3E). These observations are consistent with *MYL2* encoding for a ventricular myosin that increases expression during the maturation of hiPSC-derived cardiomyocytes. We performed validation experiments on the edited hiPSC clonal lines as per our published quality control criteria to evaluate genomic stability, pluripotency, and differentiation potential, and found that each line behaved comparably with other tagged lines (Table S1) (Coriell Medical Institute Biorepository, 2018; Roberts et al., 2017). Final clones that met our quality control criteria for the gene targets described in this report have been distributed to the public (Addgene, 2018; Coriell Medical Institute Biorepository, 2018).

Imaging Clonal mEGFP-Tagged hiPSC-Derived Cardiomyocytes Reveals Anticipated Sarcomeric Localization

Cardiomyocytes generated from clonal tagged lines were imaged both live (Figures 4D, 4F, S3A, and S3B) and after fixation and immunolabeling (Figures 4E, S3F, and S3G) by confocal microscopy. Live imaging revealed striated, sarcomeric localization of each fusion protein (Figures 4D, 4F, S3A, and S3B) with specific patterns, as expected (Figure 4A). The thick and thin filament fusion proteins from the *MYL7* and *TNNI1* experiments displayed a broader banding pattern interspersed with narrow "dark" lines where mEGFP was absent, consistent with the localization of these proteins between Z discs in myofilaments. *ACTN2* and *TTN*-mEGFP fusion proteins localized to narrow banding patterns within myofilaments, representing Z discs and M lines, respectively (Figures 4A, 4D, and 4E). The banding pattern for *TTN* was especially revealing as this protein spans the sarcomere, but C-terminal tagging results in mEGFP localization at the M line (Luther, 2009).

Antibodies specific to the tagged proteins colocalized with mEGFP, confirming anticipated colocalization of the tagged and untagged protein species within clones with monoallelic edits (Figure S3G). Unedited cells were also fixed and immunolabeled with antibodies specific to each target and showed labeling patterns that were comparable with that of the mEGFP-tagged cells (data not shown). We also confirmed expression of cTnT in edited cardiomyocytes (Figures 4B, 4C, 4E, and S3F). Most cTnT$^+$ cells were also mEGFP$^+$, indicating high penetrance of the tagged allele (Figures 4B, 4C, S3C, and S3F).

We used different criteria to evaluate *MYL2*-mEGFP because this gene is not expressed in immature hiPSC-derived cardiomyocytes, but expression increases during cardiomyocyte maturation. We observed successful cTnT expression after 12–47 days of differentiation, suggesting

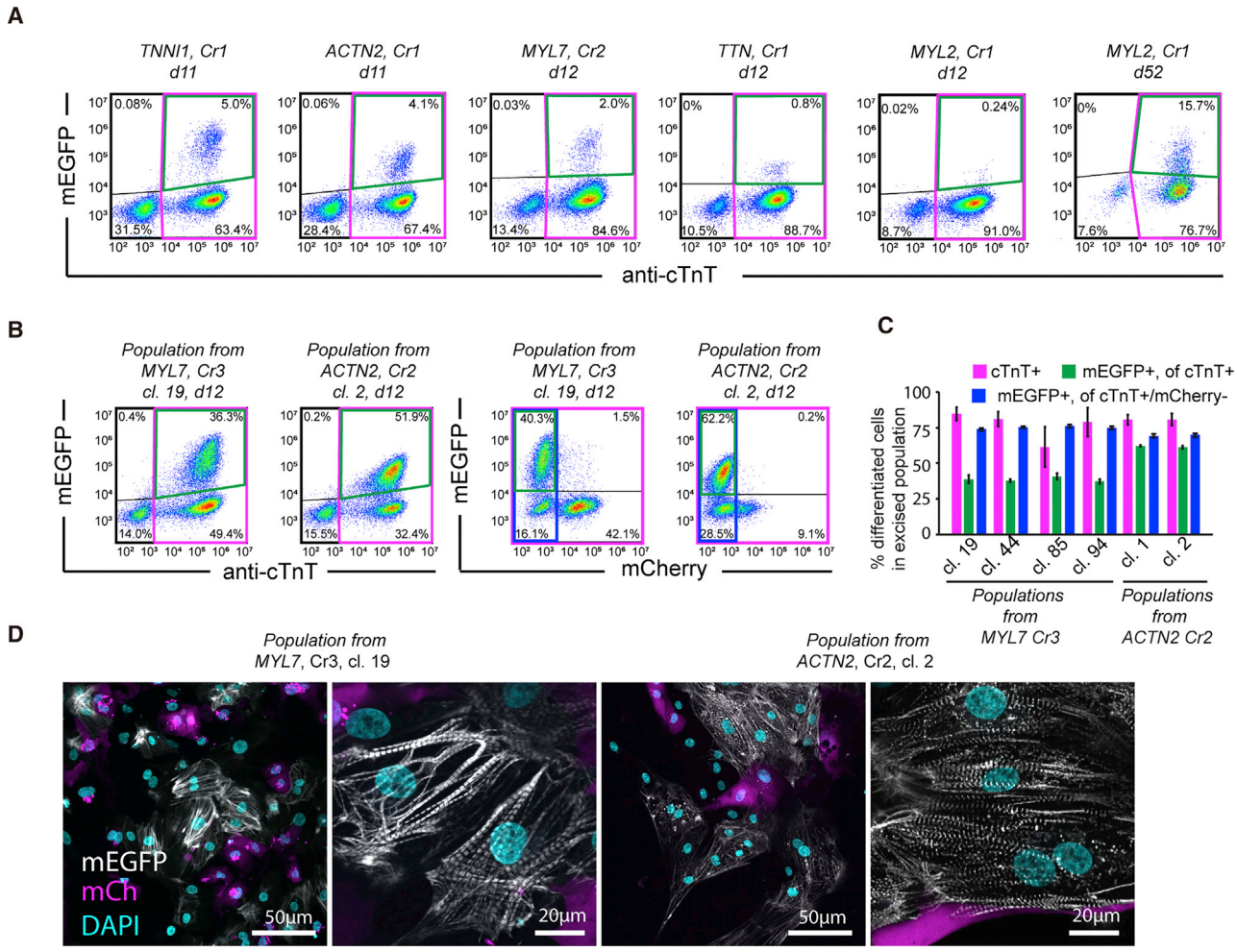

Figure 3. Flow-Cytometry and Imaging Experiments to Evaluate Tagged Allele Expression in Cardiomyocyte Cultures from Excised Populations

(A) Populations of mCherry$^-$ cells isolated after Tia1L-mediated excision of mCherry$^+$ populations with standard Tia1L RNP were differentiated into cardiomyocytes and analyzed by flow cytometry for mEGFP and cardiac troponin T (cTnT$^+$, pink box) expression (prior to clone generation, option 1). mEGFP expression was observed within the cardiomyocyte population (cTnT$^+$/mEGFP$^+$, green box, upper right quadrant). The duration of differentiation before analysis is indicated in days (d) above plots. The percentage of cTnT$^+$/mEGFP$^+$ was interpreted as an estimate of tagging efficiency.

(B) mEGFP fluorescence was plotted against antibody staining intensity (left two boxes) for the cardiomyocyte marker cardiac troponin T (cTnT, x axis), as in (A), in differentiated *ACTN2* Cr2 and *MYL7* Cr3 clones after excision with optimized RNP complex (using workflow option 2). Cells were not sorted for mCherry$^-$ cells prior to differentiation. Percentages of cells gated as positive and negative for both mEGFP fluorescence and cTnT staining are as indicated. The cTnT$^+$ population was additionally analyzed for mCherry and mEGFP expression (right boxes), revealing that most mCherry$^-$ cells are mEGFP$^+$.

(C) Flow-cytometry data from (B) was quantified among biological replicates in precisely edited unexcised clones subsequently excised with optimized RNPs, as described in (B). mEGFP expression was evaluated in all cells, cTnT$^+$ cells, and cTnT$^+$/mCherry$^-$ cells, as indicated by boxes in (B). Error bars are SD among biological replicates (n = 3).

(D) Live spinning-disk confocal microscopy of unsorted excised cells analyzed in (B) and (C). Scale bars are as indicated.

In (B) to (D), clone references are to clones genomically validated before excision (option 2).

that *MYL2* tagging did not interfere with the cardiomyocyte differentiation process (Figures 4G, 4H, and S3D). Over this same time scale the fraction of cTnT$^+$ cells expressing mEGFP gradually increased, with 25%–33% of cardiomyocytes expressing mEGFP by day 47, as detected by flow cytometry (Figures 4G, 4H, S3B, and S3E). Upon live imaging, we observed mEGFP signal in all *MYL2*-mEGFP clones localized between the Z discs in the

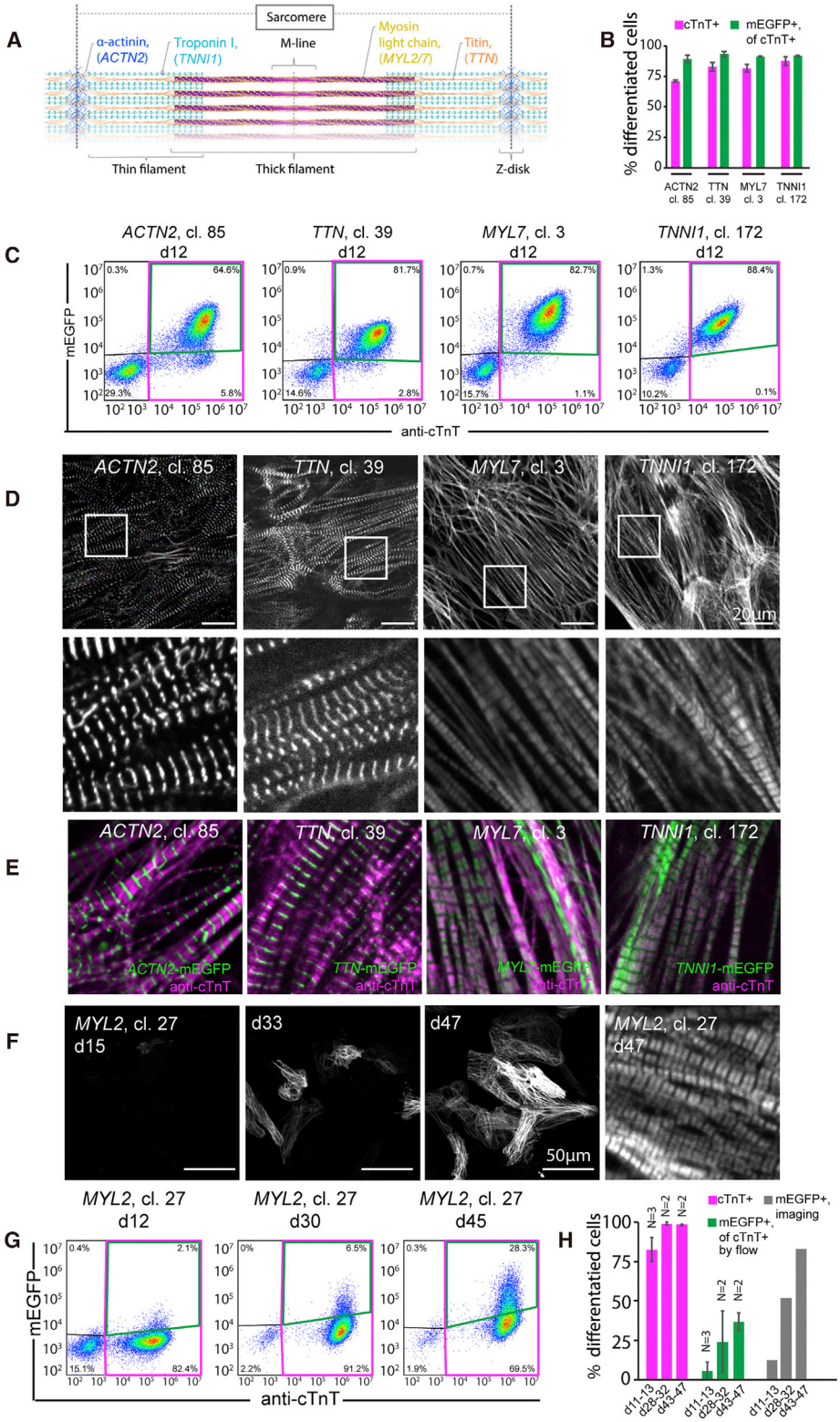

(legend on next page)

myofilament, as expected (Figures 4A, 4F, and S3B). We also observed mEGFP expression in all clones at variable intensity in an increasing fraction of cells over time (Figures 4F, 4H, S3B, and S3E). By day 47 of culture, imaging showed mEGFP expression at varying intensities in most cells (Figures 4F, 4H, and S3B). We concluded that many mEGFP-expressing cells were below the detection limit of flow cytometry but detectable with live imaging by confocal microscopy, and that each clone displayed a similar *MYL2*-mEGFP expression profile (Figures 4H, S3B, and S3E). While we tested multiple antibodies to confirm localization of *MYL2*-mEGFP-encoded fusion protein, we were unable to confirm specificity of these antibodies (data not shown).

DISCUSSION

Endogenous fluorescent tagging in hiPSCs facilitates live imaging to study the organization and dynamics of key proteins and structures. Pairing insights gained from *in vivo* studies with hiPSC-derived models will reveal mechanisms important for differentiation, development, and disease. However, such approaches require efficient strategies for endogenous tagging. To enable tagging at transcriptionally quiescent loci in hiPSCs, we targeted five non-expressed genes via HDR, enriched for putatively tagged cells with a constitutively expressed selection cassette, and generated mEGFP fusion alleles lacking genomic scars using a Cas9/MMEJ excision strategy. This approach uniquely relies on CRISPR/Cas9 for both the incorporation and subsequent excision of the selection cassette and provides the added benefits of selection without drugs, an important safeguard against potential alterations to cell integrity.

Since the use of the same Tia1L sequence drove successful and efficient excision in all experiments, this approach is likely to succeed broadly for transcriptionally silent loci. In addition, we demonstrate that adding a specific linker of choice based on known properties of the target protein, with sequence redundancy flanking the excisable selection cassette, provides a strategy to frequently achieve a desired tagging outcome. This approach could also be used to incorporate an epitope tag, cleavable peptide, mutation, or other modification. The high rate of excision observed with optimized RNPs (>77%) significantly improves the likelihood of recovering edited clones. Furthermore, this high efficiency enables a more streamlined workflow that bypasses the need for a second round of FACS and clone generation.

All precisely edited clonal cell lines generated using this method differentiated into cardiomyocytes with timely expression of the mEGFP fusion protein, demonstrating endogenous regulation and proper sarcomeric localization of the tagged protein during cardiac differentiation. The

Figure 4. Clones with Validated In-Frame Excision Events Express mEGFP Fusion Proteins with Predicted Unique Sarcomeric Localization Patterns and Dynamics after Cardiomyocyte Differentiation

(A) Schematic depicting anticipated localization of tagged sarcomeric proteins.

(B) Flow-cytometry measurements of mEGFP fluorescence and cTnT antibody staining in fixed cells differentiated for 12 days. Percentages of $cTnT^+$ cells, and $mEGFP^+$ cells within the $cTnT^+$ population, are shown in representative clones. Error is SD among biological triplicates.

(C) Flow-cytometry analysis plots used for quantification in (B) of mEGFP fluorescence (y axis) and cTnT (x axis). Most cells expressed cTnT (pink box). Within the $cTnT^+$ cell population, most cells expressed mEGFP (green box, upper right quadrant). Percentages of cells gated as $mEGFP^+$ and $cTnT^+$ are as indicated.

(D) Validated clones were differentiated into cardiomyocytes, plated on glass-bottom plates, and imaged live using spinning-disk confocal microscopy for mEGFP fluorescence. Scale bars represent 20 μm in top row; insets are 25 μm wide and additionally displayed in the lower row. *MYL2* data are shown in (F).

(E) Representative images of mEGFP signal and cTnT antibody staining indicate that mEGFP expression is observed in distinct sub-sarcomeric regions within $cTnT^+$ cardiomyocytes, based on distinct colocalization patterns. Images are 25 μm wide. All cardiomyocytes were imaged after approximately 20 days of differentiation. Staining in *MYL2* cells was not performed due to absence of a specific antibody.

(F) mEGFP expression in *MYL2*-tagged clones reveals delayed expression onset. A validated, representative *MYL2* clone with an in-frame endogenous mEGFP fusion protein was differentiated into cardiomyocytes, plated on glass-bottom plates, and imaged live. After 15–47 days of differentiation (indicated) sarcomeric mEGFP expression appeared in increasing numbers of cells and intensified. Higher-magnification image depicts the 47-day time point, demonstrating striated sarcomeric mEGFP localization. Exposure times and contrasting are equivalent at all three time points and culture wells were near confluent. A representative, precisely edited clone is shown. Scale bars, 50 μm; high-magnification image is 25 μm wide.

(G) mEGFP fluorescence in fixed *MYL2*-mEGFP cells was measured by flow cytometry (y axis) and plotted against antibody staining intensity for cTnT (x axis) as in (C). Cells were harvested for analysis after the indicated length of differentiation.

(H) Graphed data from (G) after indicated durations of differentiation. Because expression of the *MYL2*-mEGFP expression was frequently insufficient for detection by flow cytometry, percentages of $mEGFP^+$ cardiomyocytes were additionally blind counted in images such as shown in (F). Error is SD among the indicated number of biological replicates.

See also Figure S3 and Table S1.

MYL2-mEGFP hiPSC line demonstrates the utility of endogenous tagging at silent loci to enable mechanistic analyses of differentiated cells. Live imaging of *MYL2*-mEGFP cells captured the "late" expression of this myosin isoform during cardiomyocyte differentiation associated with a specific ventricular lineage. This provides a significant advantage over current methods (fixed cells) to follow the differentiation process over time. The expression and dynamic localization of each of the five sarcomeric proteins also show changes in structural organization during cardiac differentiation in live cells that can be followed during maturation. This approach should similarly enable studies of other differentiated cell types, providing a path to developing optimized methods for differentiation and maturation, tracking cell types and lineages, and studying morphogenic principles.

EXPERIMENTAL PROCEDURES

Edited cell lines, culturing protocols, experimental protocols, and hiPSC transcript abundance data from RNA sequencing is available at the Allen Cell Explorer (Allen Institute for Cell Science, 2018).

Cell Culture and WTC hiPSC Characterization

hiPSC work complied with NIH, NAS, and ISSCR Guidelines. The WTC-11 (WTC) male hiPSC line was generated by Dr. Bruce Conklin (The Gladstone Institute) (Kreitzer et al., 2013). hiPSC colonies were isolated and maintained as previously described (Roberts et al., 2017).

Donor Plasmids, crRNAs, and Cas9 Protein

We used hPGK:mCherry with the first two genes attempted (*TNNI1* and *ACTN2*) and the CAGGS:mCherry for subsequent genes. Linkers contained microhomologies such that after MMEJ, the restored sequence would function as a linker 5′ of mEGFP for each C-terminal tag. Linker sequences flanked Tia1L crRNA protospacers, which in turn flanked the mCherry expression cassette. Homology arms, genome-specific variants, and mutations to inactivate Cas9 were incorporated into donor plasmids as previously described (Roberts et al., 2017). *Streptococcus pyogenes* Cas9 protein was from the UC Berkeley QB3 Macrolab. Optimized sgRNAs were from Synthego and TrueCut Cas9 was from Thermo Fisher Scientific (#A36497). All plasmids used the mEGFP (K206A) sequence.

RNP Transfections for HDR and Excision

Cells were dissociated and transfected using the Neon transfection system as previously described (Roberts et al., 2017). Duplexed crRNA:tracrRNA was complexed in a 1:1 molar ratio with 2 μg of wild-type Cas9 ("standard RNP"), or custom Synthego sgRNAs modified with 2′-O-methyl 3′-phosphorothioate in the first and last three nucleotides of the 100-mer were complexed with 2 μg of TrueCut Cas9 ("optimized RNP" in this article). Transfected cells were cultured for 3–4 days until ~70% confluence, passaged once at 1:10, and cultured for an additional 3–4 days to allow mCherry expression from the episomal donor plasmid to decline. Negative control transfections for HDR were performed in all experiments with the crRNA targeting the AAVS1 locus (protospacer + PAM: 5′-GGG GCC ACT AGG GAC AGG ATT GG-3′) to assess the relative frequency of random donor cassette incorporation. Cells were harvested for FACS using Accutase. The Tia1L protospacer + PAM was 5′-GGT ATG TCG GGA ACC TCT CCG GG-3′. The mock sgRNA (Synthego) was 5′-gca cua cca gag cua acu ca-3′. For excision, expanded mCherry$^+$ sorted populations were dissociated into single-cell suspension and transfected as described above with Tia1L-targeting or mock RNP complexes. Transfected cells were expanded over two passages and sorted or used directly for clonal isolation or other analyses.

Flow Analysis and Sorting for HDR and Excision

Cells were sorted following HDR as described by Roberts et al. (2017). The mCherry$^+$ gate was set using mock-transfected cells. For excision, an mCherry-sort gate was set using live, mock-excised mCherry$^+$ cells. Sorted populations were expanded in GFR Matrigel-coated tissue culture plates for generation of clonal cell lines. For assessment of efficiency of enhanced editing protocols, cells were harvested with Accutase, resuspended in mTeSR1 with 1% penicillin/streptomycin (P/S) and 10 μM ROCK inhibitor, and stained with DAPI (2 μg/mL), acquired on a CytoFLEX S (Beckman Coulter) with 405-, 488-, 561-, and 638-nm lasers and analyzed with FlowJo software V.10.2 (Treestar). Doublets and dead cells were excluded based on forward-scatter (FSC)-A/H and DAPI brightness.

Droplet Digital PCR

For primary ddPCR screening, probe-based PCR amplifications were targeted to mEGFP and the two-copy genomic reference RPP30 in one multiplexed reaction and ampicillin (Amp) and mCherry in a second multiplexed reaction. Primers and hydrolysis probes are listed in the Supplemental Information. For primary screening, the ratios of ([copies/μL_{mEGFP}]/[copies/μL_{RPP30}]), ([copies/μL_{AMP}]/[copies/μL_{RPP30}]), and ([copies/$\mu L_{mCherry}$]/[copies/μL_{RPP30}]) were calculated. ddPCR was otherwise performed as described previously (Roberts et al., 2017).

Screening with Tiled Junctional PCR and Sequencing Untagged Alleles

PCR and sequencing was performed as described previously (Roberts et al., 2017) using gene-specific primers (See Table S1).

In Vitro Directed Differentiation of hiPSCs to Cardiomyocytes

Cardiomyocyte differentiation was achieved using a small-molecule differentiation with optimized small-molecule concentration and timing (Lian et al., 2015). A previously reported cytokine protocol was used to differentiate *TNNI1*-mEGFP clones (Table S1) (Gerbin et al., 2015; Palpant et al., 2015a, 2015b). In brief, cells were seeded onto GFR Matrigel-coated 6-well tissue culture plates at a density ranging from 0.125 to 0.25 × 10^6 cells per well in mTeSR1 supplemented with 1% P/S and 10 μM ROCK inhibitor, designated as day −3. Cells were grown for 3 days, with daily mTeSR1 media changes (day −2 and day −1). The following day

(designated as day 0), directed cardiac differentiation was initiated by treating the cultures with 7.5 μM CHIR99021 (Cayman Chemical) in RPMI 1640 medium (Gibco #A10491-01) containing insulin-free B27 supplement (Gibco #A1895601). After 48 h (day 2), cultures were treated with 7.5 μM IWP2 (R&D Systems) in RPMI containing insulin-free B27 supplement. On day 4, medium was replaced with RPMI containing insulin-free B27 supplement. From day 6 onward, medium was replaced with RPMI supplemented with B27 containing insulin (Gibco #17504044) every 2–3 days.

Cardiomyocyte Harvesting, Replating, and Flow-Cytometry Analysis

Wells displaying expected cardiomyocyte morphology were harvested using TrypLE Select (10×, Gibco #A1217701) diluted to 2× with Versene (Gibco #15040-066) and prewarmed to 37°C. Cells were washed twice with Dulbecco's PBS (DPBS) and incubated with 2× TrypLE/Versene for 6–10 min at 37°C. Cells were gently triturated to obtain single-cell suspension, collected into RPMI containing B27 supplement with insulin,10 μM ROCK inhibitor, and 200 U/mL DNase I (Millipore Sigma), and pelleted at 211 × *g* for 3 min at room temperature. Cells were resuspended in the same medium and counted in a hemocytometer (INCYTO C-Chip). 0.35–0.75 × 10^5 cells per well were seeded onto polyethyleneimine (PEI)/laminin-coated 24-well glass-bottom plates in RPMI containing B27 with insulin and 10 μM ROCK inhibitor. Twenty-four hours after plating, medium was changed to RPMI containing B27 with insulin and replaced every 2–4 days. Imaging was performed 5–21 days after plating. To measure cardiac troponin T (cTnT) expression, we harvested cells as described above and pelleted them at 211 × *g* for 3 min at room temperature. Cells were fixed with 4% paraformaldehyde in DPBS for 10 min at room temperature, washed once with DPBS, and resuspended in 5% fetal bovine serum (FBS) in DPBS and stored at 4°C until staining. A maximum of 5 days elapsed between fixation and staining. Fixed cells were stained for cTnT as described by Roberts et al. (2017). Cells were acquired on a CytoFLEX S (Beckman Coulter) or FACSAriaIII Fusion (BD Biosciences) and analyzed using FlowJo software V.10.2 (Treestar). To exclude doublets, we gated day-18 and younger cells using FSC-H/W and, where applicable, side-scatter-H/W. After day 19, doublets were excluded by gating with DAPI-A on the x axis and DAPI-H on the y axis, with single cells of increasing DNA content along the upsloping diagonal and aggregates below the diagonal. Gating was checked by sorting and imaging cTnT/$DAPI^+$ D12 and D30 cardiomyocytes and verifying that singlets, doublets, and multinucleated cells were obtained from the appropriate gates. The $cTnT^+$ gate included 1% of cells in the isotype control.

Imaging of Live and Fixed Cardiomyocytes

Before plating, 24-well glass-bottom plates were treated with 0.5 M glacial acetic acid (Fisher Scientific #BP1185-500) at room temperature for 20–60 min and washed once with sterile milliQ (MQ) water. Wells were treated with 0.1% PEI (Sigma Aldrich #408727-100ML) solution in sterile MQ water for 16–72 h at 4°C, then rinsed once with DPBS (Gibco #14190-144) and once with sterile MQ water. Finally, wells were incubated overnight at 4°C with 25 μg/mL natural mouse laminin (Thermo Fisher Scientific #23017-015) diluted in sterile MQ water. Laminin solution was removed immediately prior to replating. Live cell imaging was performed on a Zeiss spinning-disk microscope with a Zeiss 20×/0.8 NA Plan-Apochromat, or 40×/1.2 NA W C-Apochromat Korr UV-vis infrared (IR) objective, a CSU-X1 Yokogawa spinning-disk head, and Hamamatsu Orca Flash 4.0 camera. Fixed cell imaging was done on a 3i spinning-disk microscope with a Zeiss 20×/0.8 NA Plan-Apochromat, or 63×/1.2 NA W C-Apochromat Korr UV-vis IR objective, a CSU-W1 Yokogawa spinning-disk head, and Hamamatsu Orca Flash 4.0 camera. Microscopes were outfitted with a humidified environmental chamber to maintain cells at 37°C with 5% CO_2 during live imaging. Where indicated, cells were stained with nuclear violet (Nuclear Violet LCS1, AAT Bioquest #17543) in phenol red-free RPMI supplemented with B27 containing insulin for 10 min and washed once with identical medium without nuclear violet before images were taken.

Cardiomyocyte Immunolabeling for Imaging

Cells were fixed with 4% paraformaldehyde in PBS with 0.4% Triton X-100 (EMD Millipore #TX1568-3) for 10 min at room temperature and blocked with 1.5% normal goat serum (Vector Laboratories #S-1000-20) with 0.4% Triton X-100 in PBS for 1–3 h at room temperature. Primary antibodies were diluted in blocking solution and incubated at 4°C overnight. Secondary antibodies were diluted in blocking solution at 1:500 to 1:1,000 for 2–3 h at room temperature. DAPI (NucBlue Fixed Cell ReadyProbes Reagent; Thermo Fisher R37606) was applied for 5 min at room temperature.

Visualizing *MYL2*-mEGFP Expression in Cardiomyocytes Replated for Prolonged Culture

Cardiomyocytes were differentiated for 30–45 days, harvested, and replated onto glass-bottom plates at days 11–15 after differentiation at 0.75 × 10^5 cells per well. One plate was used for live samples and a duplicate plate was used to harvest samples for flow cytometry. Cells were harvested as described, except cells were incubated with 10× stock TrypLE Select for 10 min at 37°C. Four identically treated wells were combined for analysis.

G-Banding Karyotype Analysis

Karyotypes were analyzed by Diagnostic Cytogenetics (DCI). At least 20 metaphase cells were analyzed for both ploidy and structural abnormalities.

Testing Trilineage Potential

Each cell line was differentiated using the STEMdiff Trilineage Differentiation kit (STEMCELL Technologies) according to manufacturer's protocol. Total RNA was harvested at plating and at day 5 for mesoderm/endoderm and day 7 for ectoderm. After synthesis (Bio-Rad iScript kit) cDNA was assayed by ddPCR for (from Bio-Rad), brachyury (mesoderm), Pax6 (ectoderm), and Sox17 (endoderm). Transcript levels were normalized to *HPRT1* and compared with the transcript levels of the WTC parental line. ddPCR conditions used 58°C annealing and were otherwise identical to clone screening.

Expression of Stem Markers by Flow Cytometry

Cell dissociation was as described by Roberts et al. (2017). Cells were washed with 2% FBS in DPBS and permeabilized with 0.1% Triton X-100 and 2% FBS in DPBS for 20 min at room temperature followed by staining with anti-Nanog AlexaFluor 647, anti-Sox2 V450, and anti-Oct3/4 Brilliant Violet 510 (all BD Biosciences) for 30 min at room temperature. Cells were washed with BD Perm/Wash buffer, then 2% FBS in DPBS before resuspension in 2% FBS in DPBS for acquisition, and analyzed as described by Roberts et al. (2017).

SUPPLEMENTAL INFORMATION

Supplemental Information can be found online at https://doi.org/10.1016/j.stemcr.2019.03.001.

AUTHOR CONTRIBUTIONS

B.R. performed gene-editing design, gene editing, and genomic characterization, prepared images and figures, and wrote the manuscript. M.C.H. performed imaging and prepared images and figures. J.A. performed FACS and flow cytometry. K.A.G. performed cardiomyocyte differentiation. H.M. performed cardiomyocyte differentiation and flow cytometry and prepared images and figures. A.N. performed cardiomyocyte differentiation. J.G. performed immunolabeling and imaging experiments. C.H. performed immunolabeling and imaging. S.A.L. performed imaging. R.Y. performed immunolabeling and imaging. A.H. performed gene editing. V.V. performed genomic characterization. T.G. performed genomic characterization. M.A.F. performed genomic characterization. A.T. performed genomic characterization. S.M.R. designed experiments. R.N.G. designed experiments and wrote the manuscript. All authors contributed to experimental design, analysis, and manuscript preparation.

ACKNOWLEDGMENTS

We thank Stephanie Dinh, Colette DeLizo and Jacqueline Smith for hiPSC and cardiomyocyte culturing and preparation, Thao Do and Graham Johnson for illustrations, Irina Mueller for imaging support, and Sean Palecek for guidance. The WTC line used to create our gene-edited cell lines was provided by the Bruce R. Conklin Laboratory at the Gladstone Institute and UCSF. We thank the Allen Institute for Cell Science Founder, Paul G. Allen, for his vision, encouragement, and support.

Received: January 11, 2019
Revised: March 4, 2019
Accepted: March 5, 2019
Published: April 4, 2019

REFERENCES

Addgene. (2018). https://www.addgene.org/allen-institute-cell-science/.

Allen Institute for Cell Science. (2018). http://www.allencell.org/.

Bae, S., Kweon, J., Kim, H.S., and Kim, J.S. (2014). Microhomology-based choice of Cas9 nuclease target sites. Nat. Methods *11*, 705–706.

Coriell Medical Institute Biorepository. (2018). https://catalog.coriell.org/1/AllenCellCollection.

Dambournet, D., Hong, S.H., Grassart, A., and Drubin, D.G. (2014). Tagging endogenous loci for live-cell fluorescence imaging and molecule counting using ZFNs, TALENs, and Cas9. Methods Enzymol. *546*, 139–160.

Dambournet, D., Sochacki, K.A., Cheng, A.T., Akamatsu, M., Taraska, J.W., Hockemeyer, D., and Drubin, D.G. (2018). Genome-edited human stem cells expressing fluorescently labeled endocytic markers allow quantitative analysis of clathrin-mediated endocytosis during differentiation. J. Cell Biol. *217*, 3301–3311.

Doyon, J.B., Zeitler, B., Cheng, J., Cheng, A.T., Cherone, J.M., Santiago, Y., Lee, A.H., Vo, T.D., Doyon, Y., Miller, J.C., et al. (2011). Rapid and efficient clathrin-mediated endocytosis revealed in genome-edited mammalian cells. Nat. Cell Biol. *13*, 331–337.

Drubin, D.G., and Hyman, A.A. (2017). Stem cells: the new "model organism". Mol. Biol. Cell *28*, 1409–1411.

Gerbin, K.A., Yang, X., Murry, C.E., and Coulombe, K.L. (2015). Enhanced electrical integration of engineered human myocardium via intramyocardial versus epicardial delivery in infarcted rat hearts. PLoS One *10*, e0131446.

Gibson, T.J., Seiler, M., and Veitia, R.A. (2013). The transience of transient overexpression. Nat. Methods *10*, 715–721.

Grassart, A., Cheng, A.T., Hong, S.H., Zhang, F., Zenzer, N., Feng, Y., Briner, D.M., Davis, G.D., Malkov, D., and Drubin, D.G. (2014). Actin and dynamin2 dynamics and interplay during clathrin-mediated endocytosis. J. Cell Biol. *205*, 721–735.

Haupt, A., Grancharova, T., Arakaki, J., Fuqua, M.A., Roberts, B., and Gunawardane, R.N. (2018). Endogenous protein tagging in human induced pluripotent stem cells using CRISPR/Cas9. J. Vis. Exp. https://doi.org/10.3791/58130.

Kim, S.I., Matsumoto, T., Kagawa, H., Nakamura, M., Hirohata, R., Ueno, A., Ohishi, M., Sakuma, T., Soga, T., Yamamoto, T., et al. (2018). Microhomology-assisted scarless genome editing in human iPSCs. Nat. Commun. *9*, 939.

Kreitzer, F.R., Salomonis, N., Sheehan, A., Huang, M., Park, J.S., Spindler, M.J., Lizarraga, P., Weiss, W.A., So, P.L., and Conklin, B.R. (2013). A robust method to derive functional neural crest cells from human pluripotent stem cells. Am. J. Stem Cells *2*, 119–131.

Lackner, D.H., Carre, A., Guzzardo, P.M., Banning, C., Mangena, R., Henley, T., Oberndorfer, S., Gapp, B.V., Nijman, S.M., Brummelkamp, T.R., et al. (2015). A generic strategy for CRISPR-Cas9-mediated gene tagging. Nat. Commun. *6*, 10237.

Lian, X., Bao, X., Zilberter, M., Westman, M., Fisahn, A., Hsiao, C., Hazeltine, L.B., Dunn, K.K., Kamp, T.J., and Palecek, S.P. (2015). Chemically defined, albumin-free human cardiomyocyte generation. Nat. Methods *12*, 595–596.

Lin, S., Staahl, B.T., Alla, R.K., and Doudna, J.A. (2014). Enhanced homology-directed human genome engineering by controlled timing of CRISPR/Cas9 delivery. Elife *3*, e04766.

Luther, P.K. (2009). The vertebrate muscle Z-disc: sarcomere anchor for structure and signalling. J. Muscle Res. Cell Motil. *30*, 171–185.

Mahen, R., Koch, B., Wachsmuth, M., Politi, A.Z., Perez-Gonzalez, A., Mergenthaler, J., Cai, Y., and Ellenberg, J. (2014). Comparative

assessment of fluorescent transgene methods for quantitative imaging in human cells. Mol. Biol. Cell *25*, 3610–3618.

Nakade, S., Tsubota, T., Sakane, Y., Kume, S., Sakamoto, N., Obara, M., Daimon, T., Sezutsu, H., Yamamoto, T., Sakuma, T., et al. (2014). Microhomology-mediated end-joining-dependent integration of donor DNA in cells and animals using TALENs and CRISPR/Cas9. Nat. Commun. *5*, 5560.

Otsuka, S., Bui, K.H., Schorb, M., Hossain, M.J., Politi, A.Z., Koch, B., Eltsov, M., Beck, M., and Ellenberg, J. (2016). Nuclear pore assembly proceeds by an inside-out extrusion of the nuclear envelope. Elife *5*. https://doi.org/10.7554/eLife.19071.

Palpant, N.J., Hofsteen, P., Pabon, L., Reinecke, H., and Murry, C.E. (2015a). Cardiac development in zebrafish and human embryonic stem cells is inhibited by exposure to tobacco cigarettes and e-cigarettes. PLoS One *10*, e0126259.

Palpant, N.J., Pabon, L., Roberts, M., Hadland, B., Jones, D., Jones, C., Moon, R.T., Ruzzo, W.L., Bernstein, I., Zheng, Y., et al. (2015b). Inhibition of beta-catenin signaling respecifies anterior-like endothelium into beating human cardiomyocytes. Development *142*, 3198–3209.

Roberts, B., Haupt, A., Tucker, A., Grancharova, T., Arakaki, J., Fuqua, M.A., Nelson, A., Hookway, C., Ludmann, S.A., Mueller, I.A., et al. (2017). Systematic gene tagging using CRISPR/Cas9 in human stem cells to illuminate cell organization. Mol. Biol. Cell *28*, 2854–2874.

Sakuma, T., Nakade, S., Sakane, Y., Suzuki, K.T., and Yamamoto, T. (2016). MMEJ-assisted gene knock-in using TALENs and CRISPR-Cas9 with the PITCh systems. Nat. Protoc. *11*, 118–133.

Shen, M.W., Arbab, M., Hsu, J.Y., Worstell, D., Culbertson, S.J., Krabbe, O., Cassa, C.A., Liu, D.R., Gifford, D.K., and Sherwood, R.I. (2018). Predictable and precise template-free CRISPR editing of pathogenic variants. Nature *563*, 646–651.

Skarnes, W.C., Rosen, B., West, A.P., Koutsourakis, M., Bushell, W., Iyer, V., Mujica, A.O., Thomas, M., Harrow, J., Cox, T., et al. (2011). A conditional knockout resource for the genome-wide study of mouse gene function. Nature *474*, 337–342.

Yao, Z., Mich, J.K., Ku, S., Menon, V., Krostag, A.R., Martinez, R.A., Furchtgott, L., Mulholland, H., Bort, S., Fuqua, M.A., et al. (2017). A single-cell roadmap of lineage bifurcation in human ESC models of embryonic brain development. Cell Stem Cell *20*, 120–134.